

DIRECT IMAGING OF EXOPLANETS WITH PROJECT 1640

BRILEY LEWIS¹ UNDER THE GUIDANCE OF REBECCA OPPENHEIMER

American Museum of Natural History
Central Park West at 79th Street, New York, NY 10024, USA
CUSJ Spring 2017, Submitted April 10, 2017

ABSTRACT

Project 1640 is a suite of instrumentation and software focused on high-contrast imaging of exoplanets, probing the parameter space of companion size $> 1M_J$ and distance 5-50 AU around the host stars. The instrument consists of an apodized Lyot coronagraph, with a Mach-Zender interferometer and an integral field spectrograph, forming data cubes of dimensions right ascension, declination, and wavelength. P1640 is operated at Palomar Observatory in Southern California, in conjunction with their PALM-3000 adaptive optics system. Data reduction models out remaining speckle noise using principle component analysis and produces a residual cube, which can then be manually inspected for possible companions. For this summer project, data reduction using the Karhunen-Loève Image Projection (KLIP) algorithm was completed on many of the survey stars and inspected, in an effort to search for more candidates. At this time, two possible candidates have been found, and are awaiting further confirmation.

Keywords: data analysis, exoplanets, instrumentation, planetary systems, undergraduate

1. INTRODUCTION

In the past two decades, exoplanet science has blossomed as a field, exciting both the scientific community and the general public. The first exoplanet, 51 Pegasi b, was discovered in 1995 with the radial velocity method (Mayor & Queloz 1995), marking the start of a new age of “planet hunting.” Kepler was then launched in 2009, an entire NASA mission devoted to discovering planets based on the transit method, and to date it has revealed over 5000 candidate planets and 3000 confirmed planets (e.g. Borucki et al. 2010, and numerous others). Despite the success of these techniques, it was not until 2008 that we truly saw an exoplanet by collecting light from the object itself (Marois et al. 2008; Oppenheimer & Hinkley 2009; Traub & Oppenheimer 2011). Direct imaging of exoplanets is a feat of engineering and physics; in order to achieve the contrast needed to resolve a planet orbiting a nearby star, the instrumentation must overcome the overwhelming brightness of the star and the noise created by diffraction and scattering, both from within the optical system and from the atmosphere above. Despite these challenges, it is possible to image exoplanets, and even to extract their spectra to better understand their composition. Using all of these techniques, we now have tools to answer many questions, such as: How are planetary systems formed? What types of planets are there in the universe? How common are these planets? Are there any other habitable planets? How are brown dwarfs and planets related? How can we classify sub-stellar objects?

Project 1640 at the American Museum of Natural History aims to answer some of these questions. Started in 2008, this project is a 99-night survey at the Palomar 200-inch Hale Telescope, seeking to discover and directly image brown dwarfs and large exoplanetary companions (Hinkley et al. 2008; Beichman et al. 2010; Hinkley et al. 2011; Oppenheimer et al. 2012). The parameter space being probed by this instrument is generally a distance

from the host star on the order of 5-50 AU (where AU means “astronomical unit,” the distance between the Earth and the Sun), and of a companion mass of one Jupiter-mass (M_J) or greater. Over 200 possible target stars were chosen based on the following criteria: nearby, for higher spatial resolution; young, so that planetary companions are still self-luminous from heat of formation; and bright, since the instrumentation operates best with a greater flux of photons from the star (Beichman et al. 2010; Oppenheimer & Hinkley 2009). Of these target stars, about 150 have been observed by the team and are being processed to find possible stellar/sub-stellar or planetary companions, and even some previously undiscovered binary systems. After eight years, the survey recently came to a close as of the June 2016 observing run at Palomar Observatory, and the group is now in the process of sifting through all the data and computing statistics to come to broader conclusions about the zoo of exoplanets in the universe, including ideas about how to classify these objects.

1.1. *Why is it so Difficult to See an Exoplanet?*

The primary difficulty in directly studying exoplanets lies in the fact that planets, even young, self-luminous ones, are very faint compared to the stars they orbit and in extremely close angular proximity. For example, if we were to look at our own solar system from a distance of 10 parsecs, Jupiter would be about 10^{-8} to 10^{-12} times fainter than the Sun (depending on the wavelength of observation) and only 0.5 arcsec away. Thus both angular resolution and suppression or control of the light from the star are required to see an exoplanet (Oppenheimer & Hinkley 2009; Traub & Oppenheimer 2011).

To understand the difficulty of this, imagine first how a telescope functions. Without atmospheric distortion or imperfections in optics, a star viewed through a circular aperture, such as that of a telescope, does not appear as a single point. Instead, its “point spread function” (PSF) follows the Airy function. The PSF is the angular probability distribution of where a photon will strike the

bll2124@columbia.edu

¹Department of Astronomy, Columbia University, 550 W 120th St, New York, NY 10027, USA

image plane of an optical system, essentially describing the image formed. The Airy function, in essence, is the Fourier transform of the entrance aperture’s illumination pattern (in this case a simple, uniformly lit circle). It takes the shape of concentric “Airy rings” around the circular, bright core of the source, whose angular width in radians is roughly λ/D , where λ is the wavelength of light and D is the diameter of the telescope (Nyquist 1928). The Airy function is simply a result of diffraction of light by the telescope, an insurmountable aspect of physics (at this time).

For reference, λ/D is roughly 40 milli-arcseconds (mas) for a 5-m telescope observing at $\lambda = 1 \mu\text{m}$. In the example of viewing our solar system and trying to detect Jupiter from 10 pc away, that angular size, the limit to the resolving power of the telescope, is a mere 12 resolution elements from the Sun. The Airy rings are at that separation only about 10^{-4} times the brightness of the Sun. Thus with simple imaging techniques, Jupiter would be completely swamped by the PSF of the Sun by a factor of about a million. Simply having a perfect, reasonably sized telescope with a standard camera behind it does not permit the direct study of exoplanets (Oppenheimer & Hinkley 2009; Traub & Oppenheimer 2011).

Furthermore, most real telescopes also have a secondary mirror suspended above the primary entrance aperture that creates a central hole in the circular aperture. This modifies the Airy function in a way that brightens the Airy rings. This secondary mirror has to be supported physically, usually with beams of metal that cross the aperture in a symmetric “X” pattern. These are called “spiders” and they also induce additional, extremely bright diffraction in the form of spikes of light emanating from the central core of the image. These diffraction “spikes” have a brightness dependent on the width of the support spiders. Diffraction spikes typically have a brightness of 10^{-3} that of the star, but they are localized in the image only in the directions of the spiders themselves (typically N-S and E-W for an equatorial mount telescope).

In addition to diffraction, other real-world problems make imaging exoplanets even harder. These problems can be binned into one piece of jargon: “speckles.” Speckles come from (1) imperfections in the wave front of light entering the telescope and (2) imperfections in the optics of the telescope and whatever instrumentation is placed behind the telescope. Speckles are both dynamic and quasi-static. The atmosphere causes speckles that are stochastic and highly variable in time; while the speckles from imperfect optics are quasi-static, only affected by changes in the optical surfaces themselves, such as sagging when the telescope is rotated and the gravity vector changes, or expansion due to a change in temperature. This speckle noise currently poses one of the most significant challenges to high-contrast observations (Oppenheimer & Hinkley 2009).

Speckles appear in an image as bright dots of light, as their name suggests, roughly of the same size as λ/D scattered about the image in a seemingly random pattern (Fig. 1). Unfortunately, speckles do not behave like a typical Gaussian noise source that can be dealt with through simply collecting more data and averaging it together (as one does with long-exposure faint-

source detection in fields such as extragalactic astronomy). Rather, they exhibit statistical behavior that requires that they be controlled or eliminated in order to overcome their contribution to the background of light that a real object is being observed against (Hinkley et al. 2007; Crepp et al. 2011; Fergus et al. 2014).

Fortunately, the speckles have two properties that allow for control and elimination. First, because speckles are an optical effect due to an imperfect wave front of light used to form the final image (c.f. §2.3), one can attempt to detect and correct these imperfections optically. Second, also because they are an optical effect, their size and location in the image follows the λ/D relation mentioned above. At longer wavelengths they are larger and farther away from the star in the image, and at shorter wavelengths they are closer and smaller. Fig. 1, demonstrates this effect. A real object on the sky does not change its position simply because of the wavelength of light it is being observed with. Thus, one can discern a real object from speckles simply because it does not move when viewed in images taken at different wavelengths (Fig. 1).

Speckle Suppression Through Chromaticity

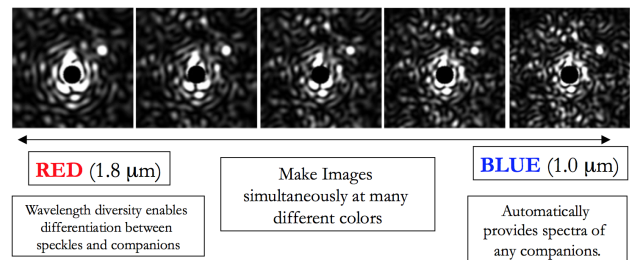


Figure 1. Four example coronagraphic images at different wavelengths from 1.0 to 1.8 μm . Speckles on the red end are further away from the star. On the blue end the same speckles are closer. The real object at top right does not move relative to the star. Thus real objects can be discerned from speckles.

2. PROJECT 1640 INSTRUMENTATION

In order to image exoplanets, Project 1640 employs several techniques to overcome the difficulties described in §1.1. For the purposes of a quick introduction, these techniques include (1) apodization and coronagraphy to control diffraction, (2) very high-order adaptive optics and precision wave front sensing to control both atmospheric and quasi-static speckles and (3) a specialized imaging device that takes images at 32 different wavelengths at once to permit discerning real objects from speckles due to the motion of speckles as a function of wavelength. A schematic of this complex suite of instrumentation is shown in Fig. 2.

First, we can significantly reduce transmission of the host star’s light by adding an apodized pupil and a Lyot coronagraph, blocking the core of the star. Wave front correction is then dealt with using adaptive optics and an interferometer, which will be further discussed in §2.3. An integral field spectrograph (IFS) is added before the detector, which aids in post-processing removal of remaining speckle noise, and also allows for low-resolution spectra to be taken from the companion objects, providing information about their compositions and more

(Hinkley et al. 2011; Oppenheimer et al. 2012).

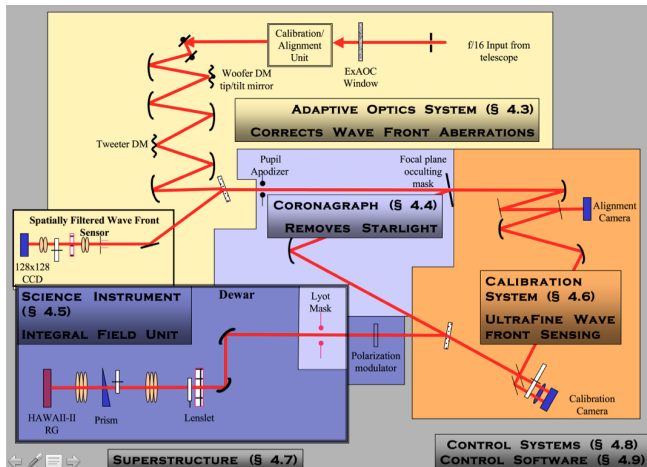


Figure 2. Summary of optical system of Gemini Planet Imager, the southern counterpart to Project 1640, which has the same components. Adapted from Macintosh et al. (2008). Section numbers here refer to documentation in Macintosh et al. (2008), not in this paper.

We describe each subsystem below by first describing control of diffraction, then control and elimination of speckles. In discussing diffraction, we will ignore speckles and assume a diffraction-limited PSF in order to describe how to suppress diffracted light in an ideal optical path. It is important to note that there are a great number of other techniques for high-contrast imaging, including speckle nulling, interferometry, and other forms of coronagraphy; the instrumentation described here is specific to Project 1640, and is closely related to that of the Gemini Planet Imager (Macintosh et al. 2014) and the ESO’s SPHERE project at the Very Large Telescope (Beuzit et al. 2006).

2.1. Apodized Pupil

To improve upon this system, a graded transmission function can be added to the telescope entrance pupil (the leftmost opening in Fig. 3) to “soften” the effects of diffraction. This “apodization” reduces the brightness of both the Airy rings and speckles, allowing the instrument to achieve higher contrasts overall (Soummer 2005; Soummer & Aime 2004; Soummer et al. 2003b,a; Oppenheimer & Hinkley 2009). The apodization optic used in Project 1640 is shown at bottom-left of the top panel of Fig. 3.

2.2. Lyot Coronagraph

Further control of diffracted light is achieved with coronagraphy. Two masks are used to obscure starlight in the Lyot coronagraph, eponymous with its inventor (Lyot 1939). The first mask is placed in the focal plane, known as the “occulting spot” or “focal plane mask.” This mask blocks out the light from the core of the star, similar to holding your thumb over a bright light to block it from your vision. The second mask is placed at the pupil plane, where it blocks some of the bright, diffraction of the focal plane mask, as well as diffraction from the secondary mirror and the spider support structure; this is the “Lyot stop” or “pupil plane mask.” The optical schematics of coronagraphy are shown in Fig. 3.

Light from a planet in the field of view is not blocked, even with the presence of the occulting spot, due to the fact that light from a planet would be coming from off the central axis. That is, it is coming in from a different spatial location from the star, and thus takes a slightly different path than the on-axis star, avoiding the occulting spot as shown in Fig. 3 (bottom panel).

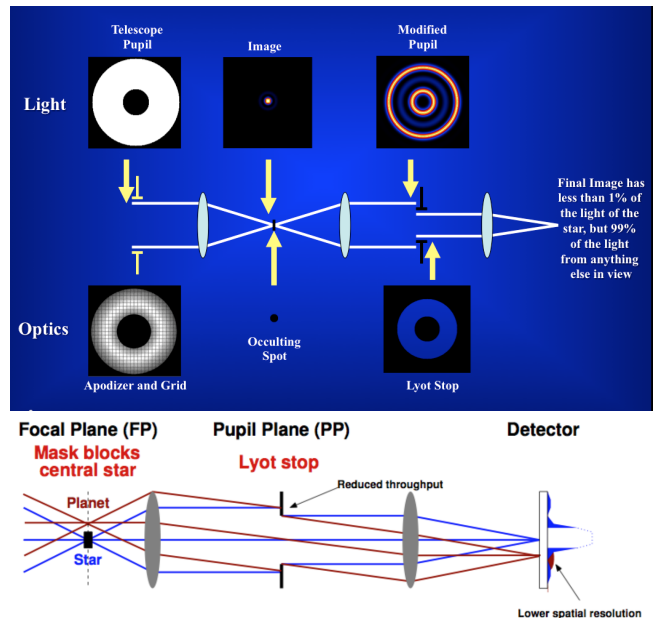


Figure 3. Top: A diagram of a Lyot coronagraph. Airy rings are visible in the “modified pupil” image. Adapted from Oppenheimer & Hinkley (2009). Bottom: Path of both “on-axis” and “off-axis” light through the coronagraph, from Kenworthy (2016).

2.3. PALM-3000 Adaptive Optics

As mentioned earlier, the wave front of a star’s light is not an ideal simple flat plane due to atmospheric turbulence, temperature differences near the telescope, and aberrations in the optics. There are imperfections, referred to as “wave front deformations,” which can significantly lessen resolution and cause speckles, reducing the contrast we can achieve with our instrument. Though the data quality is inherently somewhat dependent on the natural seeing conditions, adaptive optics systems allow for some correction of this wave front, and can bring the telescope and instrument significantly closer to diffraction-limited seeing.

Adaptive optics, using a natural guide star, works by sensing the input wave front from the target star and quickly changing the shape of a deformable mirror to counteract the deformations, ideally producing a flat wave front as shown in Fig. 4 (Oppenheimer & Hinkley 2009). The Hale Telescope’s new system, PALM-3000 (Dekany et al. 2013), has 3388 actuators controlling the two deformable mirrors, allowing them to be adjusted 2000 times per second to quickly process the incoming wave front and correct it. One of the mirrors, with around 200 actuators, deals with low-order corrections, the larger deformations in the wave front, whereas the other mirror has a much higher density of actuators for high-order corrections, the much finer details of the wave

front (Dekany et al. 2013). Additionally, there is a small tip/tilt mirror, dealing with the lowest-order corrections; it adjusts using a proportional-integral-derivative loop controller to simply keep the star at the center of the image, allowing the AO system to focus on more detailed corrections.

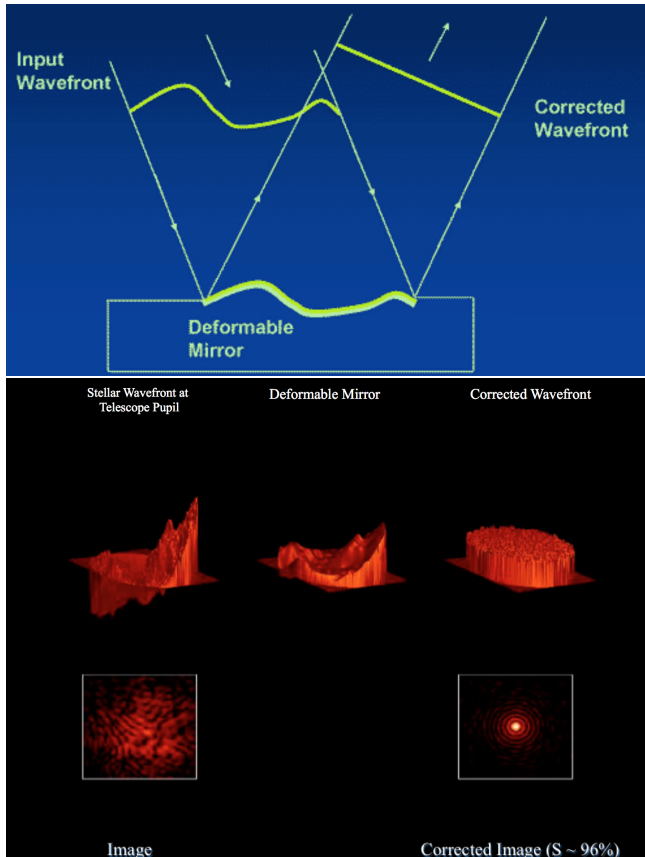


Figure 4. Top: Diagram of the basic concept of adaptive optics. Adapted from Veicht (2016). Bottom-left: simulation of input wavefront corrupted by the atmosphere, the image that results in below. Bottom-middle: shape imposed on deformable mirror. Bottom-Right: corrected wave front and below that the corrected image (courtesy J. Lloyd).

To improve upon PALM-3000, Project 1640 additionally uses a Mach-Zender interferometer, referred to as the CAL (calibration) interferometer (Zhai et al. 2012; Vasisht et al. 2012). The light rejected by the coronagraph, as well as part of the beam that will eventually travel to the IFS detector, are both processed by this interferometer, sensing any remaining deformations in the wave front down to 1 nanometer. CAL sends this information back to the PALM-3000 adaptive optics system, which then corrects for this deformation. Since CAL is placed after the coronagraph in the optics, it allows for corrections within the system, greatly improving the image and thus the achievable contrast (Oppenheimer et al. 2012; Zhai et al. 2012; Vasisht et al. 2012).

Since we have control over the deformable mirror, it is also possible to purposefully impose deformations onto the wave front, creating an image in the final science exposure. This is how “grid spots” on the data are created; these grid spots are a sinusoidal perturbation inserted into the wave front, which creates four identi-

cal images of the star outside the focal plane mask with known locations and brightness (see Fig. 5, left). The intersection of these four spots details the location of the star, which would otherwise be unknown when the star is occulted, allowing us to perform astrometry calculations and some photometry on the data if a companion is found (Sivaramakrishnan & Oppenheimer 2006; Marois et al. 2006; Oppenheimer & Hinkley 2009). In fact, the project demonstrated relative astrometry between Alcor and its newly discovered companion at a level of a few mas, allowing for parallactic motion to be used to show, within months, that the companion is indeed orbiting Alcor (Zimmerman et al. 2010). Previously companion confirmation relied upon showing that the two objects have common proper motion across the sky over years or more.

2.4. Integral Field Spectrograph

The last physical part of the Project 1640 instrument (aside from computers, electronics and software) collects the data. Project 1640 has a detector with a 3.8×3.8 arcsecond field of view, placed after an integral field spectrograph (IFS). The IFS contains an array of lenslets, which break up the incoming light into spectra, allowing us to take 32 simultaneous images in different wavelengths. Within this 2040×2040 pixel space on the detector, there are approximately 37,000 spectra, spanning the wavelength range of 995-1798 nanometers. These spectra are extracted from the raw data to form data cubes, with dimensions of right ascension, declination, and wavelength (Zimmerman et al. 2011; Oppenheimer et al. 2012).

The range of the detector falls in the near infrared, including the Y, J, and H bands. Project 1640 is aptly named, as 1640 nanometers falls within the detection range of our instrument, and in fact is the wavelength at which the system optimally suppresses a star’s light. Surveys for direct imaging of exoplanets, such as this, are conducted in the infrared because the planets we are able to image would still be glowing in the infrared from the heat of their formation. This is why our survey stars chosen are young (Beichman et al. 2010; Oppenheimer et al. 2012; David & Hillenbrand 2015).

3. DATA COLLECTION AT PALOMAR OBSERVATORY

Project 1640 has completed its 99 nights of observations over a span of 3 years at Palomar Observatory’s 200-inch (5.1-m) Hale Telescope in Southern California. This reflecting telescope, constructed in the 1940s, has been a workhorse of modern astronomy since, with notable achievements such as the discovery of the first quasar, 3C 273 (Schmidt 1963). Palomar Observatory is also where Project 1640’s own R. Oppenheimer discovered the first methane brown dwarf, Gliese 229B, in 1995, using a coronagraph on the 60-inch telescope and a spectrograph on the 200-inch telescope (Nakajima et al. 1995; Oppenheimer et al. 1995, 1998; Oppenheimer 2014).

As a part of this summer project, I had the opportunity to participate in the June 2016 observing run with the Project 1640 team at Palomar, which was incidentally the last official run of the survey. Multiple collaborators, from Johns Hopkins, Caltech, NASA JPL, Columbia University, Palomar Observatory, and the American Museum of Natural History, were also present, allowing me

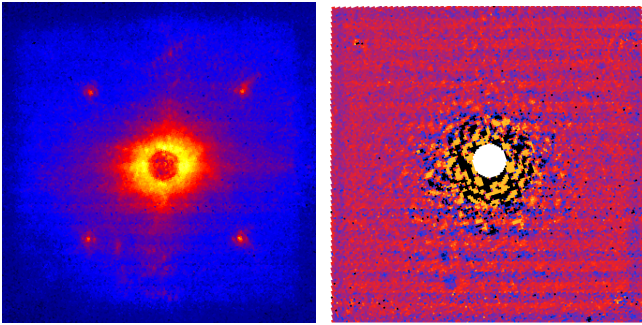


Figure 5. Examples of Project 1640 data. Left: one λ slice of a raw data cube with visible gridspots. Right: one λ slice of a residual data cube after processing using KLIP.

the opportunity to learn from each about a different aspect of this project. This experience also allowed me to participate in and directly learn about modern observational astronomy, from set-up of the instrument to actual data collection and observation logs.

4. DATA PROCESSING

Even with the complicated optical instrument described above, that is still not enough to achieve the contrasts necessary to image an exoplanet or sub-stellar companion since speckles remain in the image. In many normal astronomical contexts, this extra light would be negligible; yet, when most of the starlight has been removed, speckles become prominent features in the image, as seen in the raw data in Fig. 5, left.

This leads to the question - how can we possibly remove speckle noise? It is mostly random, unable to be accurately modeled by a physical process. Instead, we turn to the speckles themselves, using their properties and presence in one image of a data set to model them out of the other images in the data set. One important property to note is their radial movement; as speckles are mostly a result of diffraction of wave front distortions through the optics, they appear to move radially outwards with wavelength as described in §1.1. This feature is what allows spectral differential imaging (SDI), used in Project 1640 to aid in modeling out speckles, and also makes it possible to discern planets within the residual noise (Oppenheimer & Hinkley 2009).

Spectral differential imaging exploits the radial movement of speckles with respect to wavelength (see Fig. 1). This is why Project 1640 uses the IFS - to obtain simultaneous images at multiple wavelengths, so we can discern the speckles from a real object. If we scale and align all the slices of a single data cube, so that the grid spots coincide, the speckles will also be in similar positions. A planet, on the other hand, will be in different positions in each cube, since it is stationary in the original images. An algorithm can then model out the speckles, which are present in the same place in each scaled image, without modeling out the planet.

4.1. Project 1640 Data Pipeline

The method used to model speckles is referred to as PSF subtraction, since the goal is to reconstruct the point spread function of the star, including the speckles, and then subtract it from the science image, thus revealing the PSF of a fainter companion object. The KLIP (Karhunen-Loève Image Projection) algorithm is

an implementation of principle component analysis, similar to the S4 and LOCI (Locally Optimized Combination of Objects) algorithms that also reconstruct PSFs for subtraction (Soummer et al. 2012; Fergus et al. 2014). Post-processing of Project 1640 data is mainly handled by both S4 and KLIP; however, for this project, I have been reducing data with KLIP. Though it may seem redundant to reduce data twice, it is actually a powerful tool for confirming the validity of a candidate object. Since each algorithm has different strengths and shortcomings, if a candidate is visible in both outputs, that is a strong indication that it is not simply a product or error of the modeling.

Before processing data with KLIP, it is necessary to visually inspect each cube to ensure that it is of the quality needed for this survey. Since Palomar Observatory schedules specific nights for observation, instead of queue observing, some data was taken in worse seeing conditions than desired. Less than 1.4 arcsecond seeing is optimal; however, data with higher seeing values is not entirely excluded if the entire data set is under those conditions. Science exposures for this project must be fully occulted by the mask, greater than 180 seconds exposure time, with clear grid spots, and in acceptable seeing conditions. Such stringent requirements are necessary since any of these factors can prevent us from seeing a faint companion. Since KLIP also requires precise grid spots for scaling and aligning of cubes prior to running the speckle-modeling algorithm, it is necessary to fit spots to the image with an algorithm, and then visually inspect those spot fits to ensure they are correct. With spot fitting completed, the KLIP algorithm is able to scale and align the frames of the data cubes so that the grid spots coincide, then proceed with the principle component analysis speckle modeling.

4.2. Karhunen-Loève Image Projection (KLIP)

With an input of scaled and aligned data cubes, KLIP performs PSF subtraction on each cube individually, using one frame of the cube as the target image and the rest of the frames as reference images. In order to re-create the speckles of the PSF to subtract them accurately, KLIP computes principle component analysis, including a Karhunen-Loève transform, for which it is named.

In essence, principle component analysis is the process of creating an orthonormal basis that can represent the speckle noise in the data, in order to rebuild an image of that noise that is as similar to the original as possible (e.g. minimizing the difference between the image and the model). To start, the algorithm separates the wavelength slices of the input cubes into a target image $T(n)$, and a set of reference images $R_k(n)$. A whole data set (multiple cubes, generally around 10) is loaded for KLIP, so all the slices at one particular wavelength become the “target” images and the rest of the wavelengths are references. For example, an input cube has dimensions (32, 250, 250). If we input two cubes into KLIP, these dimensions become (64, 250, 250). One is chosen as the target image, so then we have one set of data with dimensions (250, 250) and another, the reference images, with dimensions (63, 250, 250). All images of the same wavelength as the target are taken out of the reference set, leaving the reference set in this case as (62, 250, 250). Some wavelengths are intentionally left out of

the reference image set to reduce contamination, so then that leaves a set of around (54, 250, 250) (J. Aguilar, personal communication, July 28, 2016).

Keep in mind that the target image can contain an astronomical signal (e.g. the point spread function of a companion) in addition to the noise, so the target image can be represented as the linear addition of the noise and an astronomical signal; our reference images are assumed not to contain the astronomical signal, implying they are images of only the noise that is to be modeled out. In order to model more accurately, KLIP segments these images into search areas, slicing the image into a specified number of annuli and sections of angle ϕ (Soummer et al. 2012).

For these search areas, the Karhunen-Loève transform is computed in order to create an orthonormal basis of eigenimages, which are basically the reference images R_p weighted by the eigenvectors of the basis c_k and normalized by the eigenvalues λ_k . The index p tracks the reference image number, n is the pixel index within the image, and k is the index of the eigenvector. A number up to K eigenvalues and eigenvectors are included in the computation. Essentially, we take a certain cutoff number of eigenimages, which are the “principle components” that make up the most of the reference image; these eigenimages are weighted by eigenvalue as to how important they are in the reference image in question. Z_k then is the weighted sum of reference images for a given eigenvector of the basis k . Smaller features are not modeled, since they are less important, e.g. less weighted by eigenvalue. This is part of why this process isn’t entirely exact, and can’t get rid of all speckles in a given image.

$$(Z_k)^{KL} = \frac{1}{\sqrt{\lambda_k}} \sum_{p=1}^K c_k(\psi_p) R_p(n)$$

Additionally, given an infinite number of references, it would be possible to find a basis that exactly represents the input data; however, we are limited to at most the $p = 31$ slices of each cube, not including the frame selected as a target image, so our basis is only an approximation. This process can be visualized for the first four eigenimages of an arbitrary reference image in Figure 6.



Figure 6. Reconstructed image with its eigenimages, weighted by eigenvalue. (Image from a talk by Václav Hlaváč)

However, not all eigenimages should necessarily be included - fewer modes (e.g. number of eigenimages included) can lead to under-modeling, not subtracting enough of the noise to see a faint object, but too many KL modes can lead to over-modeling, subtracting out any signal from the objects we are searching for (Soummer et al. 2012). To compensate for this uncertainty, KLIP is run with a variety of parameters (annuli, angular sections, KL modes) over each image. This produces multiple outputs, including a “median-combined” image,

which averages the residual outputs of all KL-mode options for a given set of annuli and angular sections.

Following computation of Z_k for each eigenvector, T is projected onto Z_k for all pixels n in the image, giving a measure of the similarity between the two images. The weighted sum of reference images itself is multiplied by this product, weighting it by importance in the final sum for the reconstructed PSF $I(\psi_0)$. This is repeated for each eigenvector k in the basis.

$$I(\psi_0) = \sum_{k=1}^K \langle T, (Z_k)^{KL} \rangle (Z_k)^{KL}(n)$$

Given this model, PSF subtraction can finally be done, creating a final residual image $F(n)$ (Soummer et al. 2012).

$$F(n) = T(n) - I_{\psi_0}(n)$$

4.3. Planetary Detection

In order to detect planets and other companion objects in the data, it is necessary to again exploit the radial motion of the speckle noise. When viewing the residual data cubes after using KLIP, or other PSF subtraction algorithms, the remaining speckles that have not been modeled out generally still appear to move. An exoplanet, on the other hand, would not share that property of radial motion, and can be seen as the one fixed object in the image. Attempts have been made at automating this data searching with an algorithm, but at this time the human eye is still superior.

4.4. Signal-to-Noise Ratio Maps

In addition to visual inspection of raw data cubes, signal-to-noise ratio (SNR) maps can be useful for more easily distinguishing a candidate object from the background. In our residual data cubes, the pixel values should approximately follow a Gaussian, with the distribution centered at zero, due to details of the KLIP algorithm that produces the processed data cubes. Additionally, the pixel values tend to fall off radially in the residual cubes, due to the fact that the majority of noise from the host star is concentrated at the center, where the host star is physically located in the image. These properties can be harnessed to judge the significance of a detection; essentially, we are trying to see where the planetary signal falls on this Gaussian of pixel values. If the pixels fall within one standard deviation, they are likely from this same distribution of the noise. For example, if they are three standard deviations away (a “3 sigma detection”), then we can judge that they may arise from a different distribution altogether and are therefore significant. By looking at standard deviations, we can judge the confidence with which we can claim a detection; a one-sigma detection implies that there is an approximately 68% chance the object is not from the noise. Three-sigma detections are more accepted as valid, however, as they imply a 99.7% chance the object is not a part of the noise.

Signal-to-noise ratio maps are one way of judging the significance of a detection based on the standard deviation of the pixel values in the image. We assume that

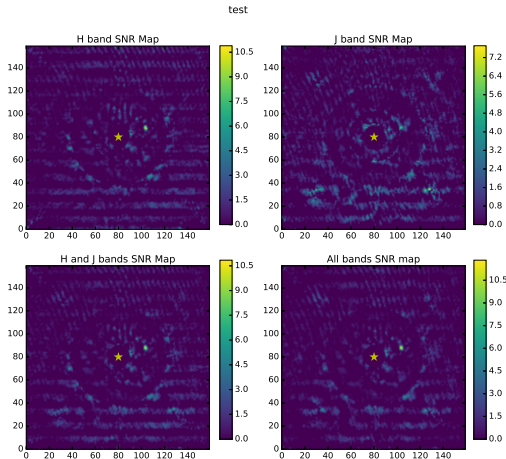


Figure 7. Example SNR map, for a “test” object. Companion is clearly visible near upper right limb of the star.

the noise is the one-sigma value of the pixel value distribution, and then divide all pixels in the image by this value to calculate the “signal-to-noise ratio”. In theory, a significant detection should stand out as a bright spot in this sort of map, where the signal is significantly higher than the noise. With a value seen over this threshold, we could claim a one-sigma detection. One sigma is not a particularly high confidence level, but is good enough for a preliminary look at the data, which is all this technique aims to accomplish. To claim a more conclusive detection, we would need to reach towards the three to five sigma level and use more complex methods.

5. RESULTS

Approximately 40 out of the 150 survey stars have been processed with KLIP as a part of this summer project. Much of the data processed is marginal, in seeing or weather conditions that are not ideal, or with less than a full set of data (considered to be 60 minutes or more of observation time). One prospective candidate object has been discovered, very close to our detection limits². It only appears in four pixels in the residual data cubes processed with KLIP, from an observing run in July 2015, and is visible in multiple wavelength bands. There is currently only one epoch of Project 1640 data on this star, and a second epoch of observation was completed in August at the W.M. Keck Observatory in Hawaii with some of our collaborators; however, this data was of marginal quality, and was not able to give us additional information. This star is on the list for re-observation in P1640’s final follow-up run at Palomar Observatory in April 2017.

Additionally, a second possible companion has been discovered around a different star. Though originally noticed in a reduction processed with the S4d algorithm, it is also now seen in a reduction done with KLIP as a part of this summer project. It is visible in multiple wavelength bands throughout the data cube, and appears to be fairly large, especially in comparison with the other possible companion mentioned above. There is only one

² Names of these objects are omitted from this paper, as more work is needed before we announce any possible discovery. Papers in preparation are not noted since we are still in the early stages, but are in progress for some candidates.

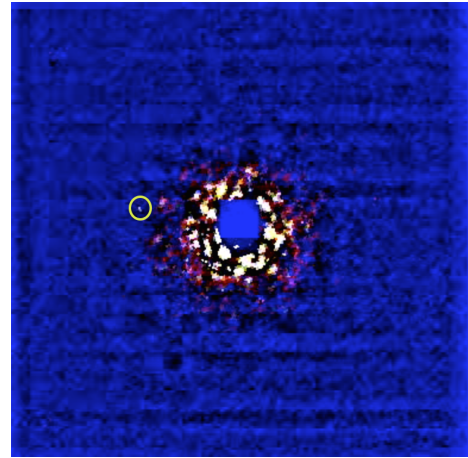


Figure 8. First possible companion (circled) around an occulted star in a KLIP-processed data cube.

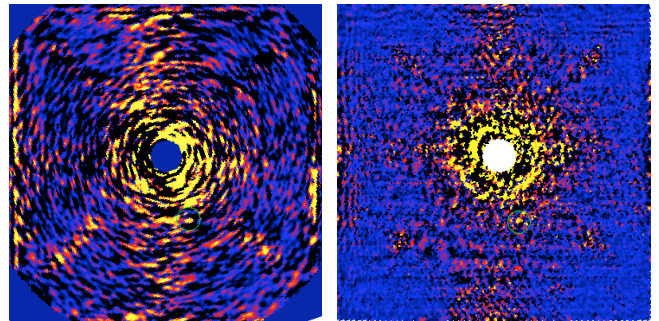


Figure 9. Second candidate companion (circled). Left: slice of the residual data cube, processed with S4. Right: slice of the residual data cube, processed with KLIP.

epoch of P1640 data on this star as well, from April 2015. To follow up on this object, other members of the team are extracting a spectrum from this object using the S4s algorithm. If the spectrum indicates it is a viable candidate, we plan to re-observe when it is visible again in April 2017.

Lastly, a third possible companion has been discovered around yet another star. First observed in July 2015, this object was observed again in October 2016. Both epochs of data, as well as the signal-to-noise ratio maps for each, clearly show the presence of a large bright spot at least 1σ above the noise. Based on preliminary astrometric estimates, this object is moving opposite the direction of expected motion of a background star, indicating it may be gravitationally bound to its host star. With more detailed calculations, we hope to further constrain some of its orbital parameters to ensure that it is a physically plausible system. A spectrum is in preparation and should provide more detail on this object as well.

6. DISCUSSION

Based on reductions of other data, there is a possibility the first candidate is an artifact of either the detector itself or the KLIP reduction process. Similar bright pixels have appeared in multiple data sets at nearly the same coordinates and in similar slices of the cube, but not exactly identical. Additionally, we have not yet been able to see this same possible companion in reductions with S4 (example shown in Fig. 11), so a spectrum will have

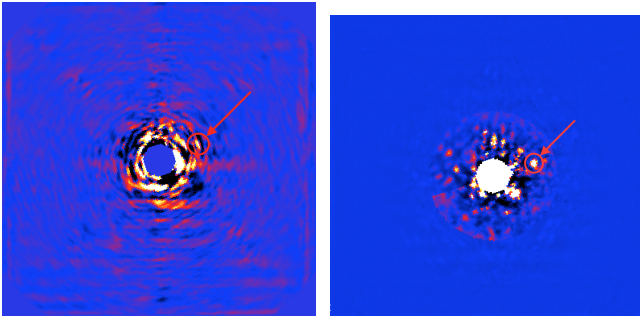


Figure 10. Third candidate companion (circled). Left: slice of the residual data cube, processed with S4. Right: slice of the residual data cube, processed with KLIP.

to be obtained through other methods, such as aperture photometry, to investigate this issue further. The lack of detection in S4 does raise doubt about the credibility of this object, but that is not a strong enough indication to completely disregard this object as a false positive.

The second and third candidates, however, seem greatly promising, given their clear visibility in both data reductions and in the signal-to-noise ratio maps. Spectra are required for further work on these objects, however, and a second epoch of data is needed for candidate two and will hopefully be obtained at the April 2017 observation run at Palomar.

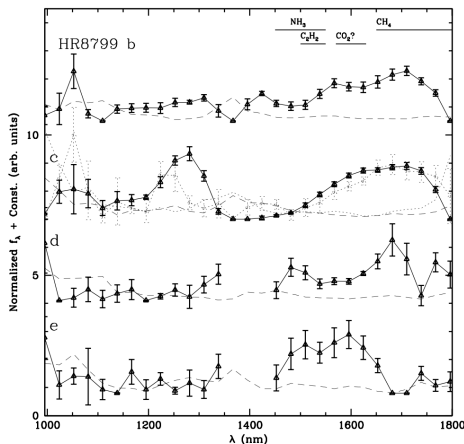


Figure 11. Example of four spectra extracted using the usual S4 methods of Project 1640. (Oppenheimer et al. 2013)

7. CONCLUSION

Though there are many possible pitfalls in the complicated, new world of direct imaging, the possibility of three new directly imaged planets is extremely exciting. Few planets have yet to be discovered by direct imaging, though the technique has been proven to work by imaging known systems, such as that of HR8799. As the technology improves, this technique seems promising for unveiling important and interesting information about extrasolar systems.

These new direct imaging surveys such as Project 1640, Gemini Planet Imager, SPHERE, and others mark a new age of astronomy and high-contrast imaging, which is the result of years of innovation in instrumentation, mechanical engineering, optical systems, data processing algorithms, and more. Though so far we have not

discovered as many planets with direct imaging as originally expected, those that have been revealed through all methods of detection topple the preconceptions of what a planetary system is expected to look like. Hot Jupiters, circumbinary planets, and many other objects already discovered represent the great diversity of planets, and are simply the tip of the iceberg for what exists for scientists to discover. The next few decades should be a time of great excitement and revolutionary thought, answering questions about how solar systems form and planets migrate, how to define the wide range of sub-stellar objects in existence, and even how to find prospective habitable planets and life on other worlds.

This paper is based on observations obtained at the Hale Telescope, Palomar Observatory. This work was funded through the National Science Foundation Research Experiences for Undergraduates program. The author would also like to thank the rest of the Project 1640 team for their support and guidance over the course of this internship, especially Rebecca, Jonathan, Emily, Ricky, Aaron, and Statia, as well as all those who made the 2016 AMNH REU possible.

Facilities: Hale (Project 1640)

REFERENCES

- Beichman, C. A., Krist, J., Trauger, J. T., et al. 2010, *PASP*, 122, 162
- Beuzit, J.-L., Feldt, M., Dohlen, K., et al. 2006, *The Messenger*, 125, 29
- Borucki, W. J., Koch, D., Basri, G., et al. 2010, *Science*, 327, 977
- Crepp, J. R., Pueyo, L., Brenner, D., et al. 2011, *ApJ*, 729, 132
- David, T. J., & Hillenbrand, L. A. 2015, *ApJ*, 804, 146
- Dekany, R., Roberts, J., Burruss, R., et al. 2013, *ApJ*, 776, 130
- Fergus, R., Hogg, D. W., Oppenheimer, B. R., Brenner, D., & Pueyo, L. 2014, *ApJ*, 794, 161
- Hinkley, S., Oppenheimer, B. R., Brenner, D., et al. 2008, in *Society of Photo-Optical Instrumentation Engineers (SPIE) Conference Series*, Vol. 7015, Society of Photo-Optical Instrumentation Engineers (SPIE) Conference Series, pp. 701519–701519–10
- Hinkley, S., Oppenheimer, B. R., Soummer, R., et al. 2007, *ApJ*, 654, 633
- Hinkley, S., Oppenheimer, B. R., Zimmerman, N., et al. 2011, *PASP*, 123, 74
- Kenworthy, M. 2016, PhD thesis
- Lyot, B. 1939, *MNRAS*, 99, 580
- Macintosh, B., Graham, J. R., Ingraham, P., et al. 2014, *Proceedings of the National Academy of Science*, 111, 12661
- Macintosh, B. A., Graham, J. R., Palmer, D. W., et al. 2008, in *Presented at the Society of Photo-Optical Instrumentation Engineers (SPIE) Conference*, Vol. 7015, Society of Photo-Optical Instrumentation Engineers (SPIE) Conference Series, 701518–701518–13
- Marois, C., Lafrenière, D., Macintosh, B., & Doyon, R. 2006, *ApJ*, 647, 612
- Marois, C., Macintosh, B., Barman, T., et al. 2008, *Science*, 322, 1348
- Mayor, M., & Queloz, D. 1995, *Nature*, 378, 355
- Nakajima, T., Oppenheimer, B. R., Kulkarni, S. R., et al. 1995, *Nature*, 378, 463
- Nyquist, H. 1928, *Transactions of the American Institute of Electrical Engineers*, Volume 47, Issue 2, pp. 617–624, 47, 617
- Oppenheimer, B. R. 2014, in *Astrophysics and Space Science Library*, Vol. 401, 50 Years of Brown Dwarfs, ed. V. Joergens, 81
- Oppenheimer, B. R., & Hinkley, S. 2009, *ARA&A*, 47, 253
- Oppenheimer, B. R., Kulkarni, S. R., Matthews, K., & Nakajima, T. 1995, *Science*, 270, 1478
- Oppenheimer, B. R., Kulkarni, S. R., Matthews, K., & van Kerkwijk, M. H. 1998, *ApJ*, 502, 932

- Oppenheimer, B. R., Beichman, C., Brenner, D., et al. 2012, Society of Photo-Optical Instrumentation Engineers (SPIE) Conference Series, 8447
- Oppenheimer, B. R., Baranec, C., Beichman, C., et al. 2013, *ApJ*, 768, 24
- Schmidt, M. 1963, *Nature*, 197, 1040
- Sivaramakrishnan, A., & Oppenheimer, B. R. 2006, *ApJ*, 647, 620
- Soummer, R. 2005, *ApJ*, 618, L161
- Soummer, R., & Aime, C. 2004, in *Advancements in Adaptive Optics*. Edited by Domenico B. Calia, Brent L. Ellerbroek, and Roberto Ragazzoni. Proceedings of the SPIE, Volume 5490, pp. 495-503 (2004)., ed. D. Bonaccini Calia, B. L. Ellerbroek, & R. Ragazzoni, 495–503
- Soummer, R., Aime, C., & Falloon, P. E. 2003a, in *EAS Publications Series*, ed. C. Aime & R. Soummer, 93–105
- Soummer, R., Aime, C., & Falloon, P. E. 2003b, *A&A*, 397, 1161
- Soummer, R., Pueyo, L., & Larkin, J. 2012, *ApJ*, 755, L28
- Traub, W. A., & Oppenheimer, B. R. 2011, *Direct Imaging of Exoplanets* (University of Arizona Press), 111–156
- Vasisht, G., Cady, E., Ligon, E. R., et al. 2012, *PASP*, submitted
- Veicht, A. 2016, PhD thesis, Columbia University
- Zhai, C., Vasisht, G., Shao, M., et al. 2012, in *Society of Photo-Optical Instrumentation Engineers (SPIE) Conference Series*, Vol. 8447, 259
- Zimmerman, N., Brenner, D., Oppenheimer, B. R., et al. 2011, *PASP*, 123, 746
- Zimmerman, N., Oppenheimer, B. R., Hinkley, S., et al. 2010, *ApJ*, 709, 733